Essential Readings in Light Metals: Electrode Technology for Aluminum Production.
Edited by Alan Tomsett and John Johnson.

Light Metals — From ***Light Metals 2011***, Stephen J. Lindsay, Editor

REAL TIME TEMPERATURE DISTRIBUTION DURING SEALING PROCESS AND ROOM TEMPERATURE AIR GAP MEASUREMENTS OF A HALL-HÉROULT CELL ANODE

Olivier Trempe[1], Daniel Larouche[2], Donald Ziegler[3], Michel Guillot[2], Mario Fafard[1]

[1]NSERC/Alcoa Industrial Research Chair MACE[3] and Aluminium Research Centre-REGAL, Laval University, Sciences and Engineering Faculty, Adrien-Pouliot Building, Québec City, Canada, G1V 0A6
[2]Aluminium Research Centre-REGAL, Laval University, Sciences and Engineering Faculty, Adrien-Pouliot Building, Québec City, Canada, G1V 0A6
[3]Alcoa Canada, 1 blvd. des Sources, Deschambault-Grondines, Qc, G0A 1S0, Canada

Keywords: anode, cast iron, temperature, thermocouple, air gap, metallography, Hall-Héroult

Abstract

An experimental investigation of the sealing process of an anode assembly used in electrolysis cells has been performed to better define the thermal and mechanical aspects of the cast iron thimble solidification between the steel stub and carbon hole. Three holes of a baked anode have been thoroughly measured with a Coordinate Measuring Machine (CMM) to obtain a high precision three-dimensional map of the carbon interface. These measurements were then compared to the outer surface of the frozen thimbles to obtain a room temperature air gap dimension. Thirty-nine thermocouples, placed in a strategic configuration, allowed the reconstruction of the temperature field in the steel stub, carbon block and solidifying cast iron thimble from the pouring to room temperature. Hence, heat transfer coefficients can be evaluated at the carbon/cast iron and steel/cast iron interfaces with a thermal model. Metallographic analysis is matched with the cooling curves.

Introduction

Prediction of the initial air gap in an anode is of high interest for people who aim at modeling the thermo-electro-mechanical behavior not only of an anode but also the whole aluminium electrolysis cell. It is a key parameter that defines the quality of thermal and electrical contact at the connection, thus influencing the voltage drop and current distribution in the anode and cell.

In the recent years, many attempts have been made to model the anode with generally satisfactory results [1-5] using a simple relation proposed by Richard [4] to predict the air gap :

$$\gamma = r_{stub} \times \alpha_{steel} \times (T_a - T_0)$$
$$gap = \gamma + (l - \gamma) \times \alpha_{iron} \times (T_s - T_0) \quad (1)$$

Where, T_a is the steel temperature at the moment of the cast iron solidification, T_s is the solidification temperature of cast iron, l is the cast iron thickness and α are the thermal expansion coefficients.

However, no actual measurements have been made in an industrial environment to assess the quality of the predictions made by this relation.

This current work is an effort to provide crucial information to validate a 3D thermo-mechanical solidification model of an anode sealing process. Within this scope, the following results are presented :

- Measurements of the air gap at the carbon/cast iron interface;
- Measurements of the temperature field during the sealing process;
- Metallographic analysis of the cast iron;
- Evaluation of the heat transfer coefficients at the interfaces;

Air gap measurement methodology

Two different methodologies, both with their advantages and disadvantages have been considered to measure the air gap. Real-time measurements with Linear Variable Displacement Transducers (LVDT) have been extensively used in experimental setups [6-12] and allows tracking the opening of the air gap as the molten metal solidifies and cools down. It is therefore an easy task to estimate the Heat Transfer Coefficient (HTC) at the interface as a function of gap opening and temperature along with thermocouple measurements so the method serves well for numerical model validation. The second method, differential measurements, doesn't yield a real time air gap magnitude but rather a final value at room temperature. Three-dimensional measurements of the stub holes and cast iron thimbles are compared to obtain the air gap. The latter method has been chosen for reasons of logistics and simplicity.

The stub holes are measured prior to casting with a coordinate-measuring machine (CMM) by taking over 2000 points spread over equally spaced heights along the interior surface of each hole. The spatial coordinates of each point are stored in the CAD drawing file of the stub hole, indicating their position with respect to the theoretical surface. The same process is used with the frozen iron after is it withdrawn from the stub hole. The two sets of measurements are aligned with a best fit method and the air gap is computed locally from the sum of the deviation of the measured coordinates versus the CAD coordinates.

CMM stub hole and thimble measurements

Because of its bulky size and weight, the anode was mounted sideways next to the CMM as shown in Figure 1. An extension was used so the probe could reach the stub holes.

A parametric Computer Numerical Control (CNC) program controls the CMM and the work is done with an automated procedure. The probe has a target measuring point corresponding to the CAD surface and an approach vector which is perpendicular to the surface. It records the actual measured point and its

deviation from the stored drawing. Figure 2 shows a 3D representation of the measured points. The green ones are within an arbitrary tolerance compared to the CAD.

Figure 1 : Set-Up of the stub holes measurements with the CMM

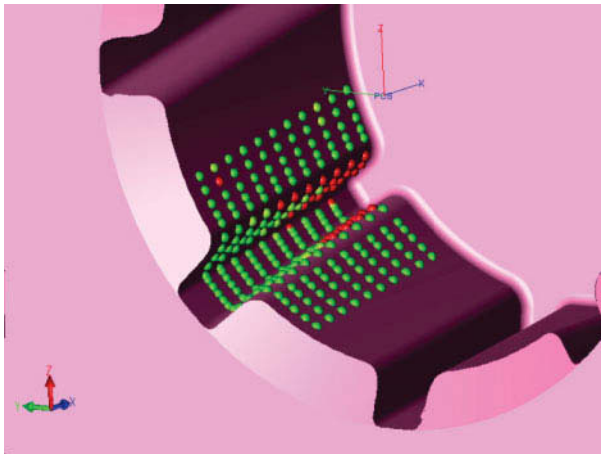

Figure 2 : 3D representation of a stub hole measurements

A complete three stub assembly was not used for the experiments but rather three separated stubs allowing for good alignment in the holes and a clean surface. The cast iron usually cracks when cooling due to stress arising as the thimble shrinks around the stub. During the withdrawal of the thimbles and stubs from the carbon, the first thimble fell apart from its stub because it was cracked. As a precaution, the two other ones were tack welded to ensure that the assembly remained in one piece. Figure 3 shows the measurement of one thimble following the same procedure as the stub holes except that the approach vectors are inverted.

Air gap dimension

Figure 4 contains the results computed locally in the cylindrical part of the thimble number 2. The magnitude is scaled for reasons of confidentiality. The position refers to equally spaced heights in the stub hole, position 0 being the top of the hole and position 11 being the bottom. All the locally computed gaps around the stub hole are represented as data points and the average gap is plotted as a line. Many measured points have been excluded from the analysis because of their obvious incongruity, that is, negative or excessive magnitude.

Figure 3 : Measurements of the cast iron thimble

A clear trend appears as the air gap is smaller in the bottom section of the stub hole. This is in agreement with the fact that the hole has a tapered profile over the height, thus resulting in the cast iron section being thicker in the upper part of the thimble. It is therefore expected to observe a larger gap in the upper part because of thermal shrinkage.

The results were compared with the predicted gap given by the Richard's relation, Equation (1). Confidentiality does not allow quantifying the difference but it can be said that the relation underestimates the magnitude of the air gap.

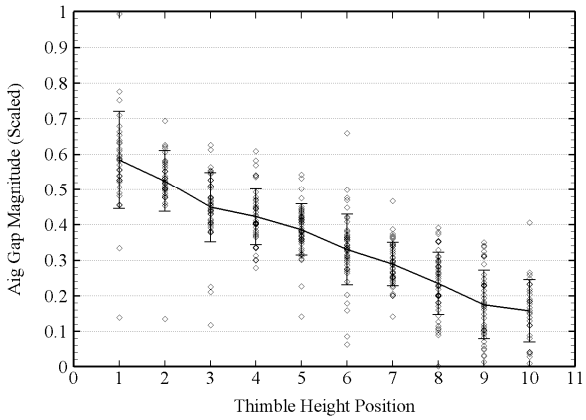

Figure 4 : Scaled air gap magnitude as a function of height in the cylindrical part of stub hole number 2

Choice of thermocouples

The molten cast iron is poured in the anode at temperatures rising up to approximately 1350°C depending on the circumstances of the process. As a first approximation, it is fair to expect the cast iron will solidify within two minutes, considering that the anodes are suspended from the transport conveyor in the plant within two minutes of pouring.

It therefore important to use thermocouples (TC) well adapted to the process to be investigated, that is, resistant to high temperature, fast response time and small thermal inertia in order not to disturb the temperature field. Unsheathed tip, 24 gauge, 3.175mm bead, type K and type S TCs were chosen for the experiments based on preliminary trials conducted for qualification purpose.

Thermocouple configuration

Thirteen TCs have been placed in each stub hole, giving a total of thirty-nine measurement points. Holes drilled in the baked anode and steel stub allow insertion of the TCs at the desired location in the steel, carbon and cast iron. Figure 5 shows the configuration for the whole anode with the following notation: A letter referring to the material in which the TC is (Cast **I**ron, **S**teel, **C**arbon), a number to identify the position of the TC and a second number identifying the stub hole.

Sets of TCs are placed on a radial pattern at two different heights, that is, at one and two third of the depth of the stub holes. Two TCs are placed in the cast iron halfway between the two interfaces in the cylindrical part. Two TCs are in one fin of the thimble. Two TCs are placed 1 cm inside the steel surface and four TCs are in the carbon 2 and 8.5 cm away from the interface. In addition to that, there are three TCs placed in the middle of the steel stub distributed over the height. A silver compound has been used to ensure a good thermal contact between the thermocouple and the surfaces.

The data acquisition is performed with a DataTaker® DT85 for a period of 24 hours after the time of the anode casting. The data logger records one data point per TC per second.

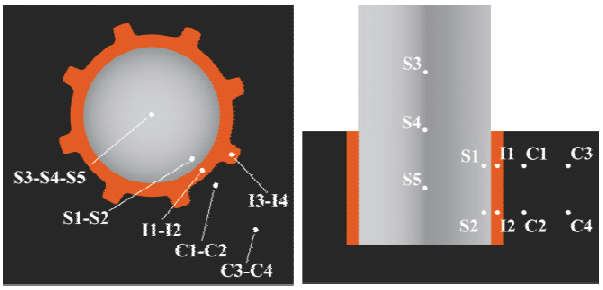

Figure 5 : Thermocouple configuration in a stub hole

Thermocouples results

The casting was carried out with a single crucible, thus there was a time lag between the corresponding curves for each hole as the first stub to be cast was the right one (3) and the casting ended with the center one (2). The superimposition of the curves was adjusted with the moment the molten iron touched the TCs.

Cast Iron

The first 350 seconds of the cooling curves of the cast iron are presented in Figure 6. From the numbering shown in Figure 5, the solid lines are the TCs in the cylindrical part and the dashed lines are the TCs in the fins. Thick and thins lines represent the high and low locations of the TCs.

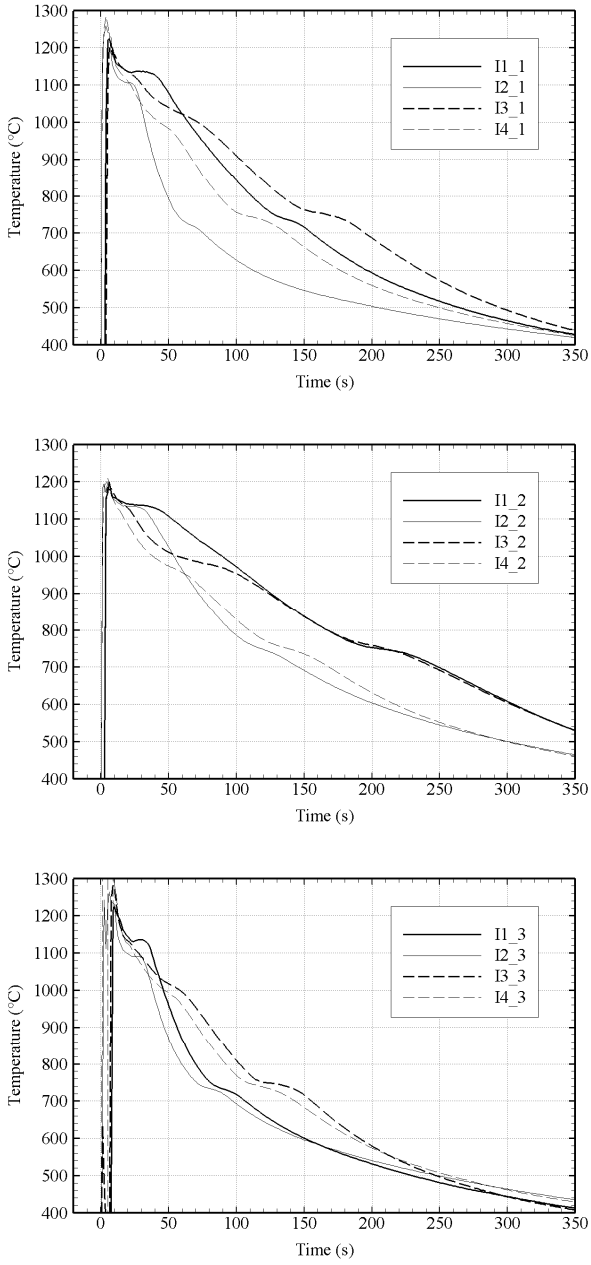

Figure 6 : First 350 seconds of the temperature recorded in the three cast iron thimbles during sealing

There is an appreciable difference between the corresponding curves of the three holes. Some hypotheses are formulated to explain this observation. The casting was made in an industrial environment so some parameters could not be controlled as would have been possible with an entirely experimental setup. The stubs and TCs were placed in the holes with great care to alignment and centering but imprecision in the order of a millimeter was likely to occur. In addition to that, having three holes in an anode with random fins orientation makes it impossible to have the same

boundary conditions for every hole. Also, the filling rate and mass were not controlled. It resulted the center hole (2) being overfilled. The heterogeneous state of the carbon material can also have an influence on the thermal field.

The casting sequence (3,1,2) can be deduced by the maximum temperature recorded. The stub hole 3 has a maximum temperature of almost 1300°C and the stub hole 2 doesn't exceed 1200°C. The cast iron was heated up to 1485°C in an induction furnace, transferred into a crucible and brought to the anode to be cast. In each of these steps, heat was lost and it explains the maximum temperature difference. The slight time lag between the thick and thin lines at 0s is the time taken to fill the cavity to reach the two highest TCs.

It is obvious that the cooling is slower in the fins and in the higher part of the stub holes as the I3 TC is generally the slowest to cool down and the I2 TC is the fastest.

The latent heat released by the phase changes during cooling is easily observable with two major plateaus in all the curves: one at around 1150°C associated with the formation of the austenite and one at around 750°C being the eutectoid reaction. However, two different behaviors can be observed depending on the TC locations. The curves representing the cooling in the fins, in which there is more mass, have a steadier and slower cooling rate and there is a subtle slope variation between 1050 and 1000°C suggesting there is another phase change there. The same behavior is not recorded by the TCs in the cylindrical part of the thimble. It also appears in thimble 1 and 3 that the thinner section (TC I2) experienced undercooling at the austenite formation temperature. Metallographic analyses presented in the next section confirm that a different solidification path was followed by the iron at the different locations.

Carbon and Steel

The curves recorded in the carbon (Figure 7) and steel (Figure 8) show a similar pattern to the three holes and for reasons of conciseness, only the curves for stub hole 1 are presented here. The differences between holes can be attributed to the same hypotheses stated in the previous section.

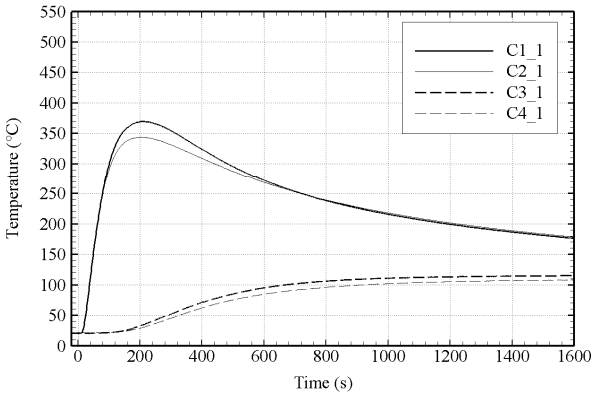

Figure 7 : First half hour of the temperatures recorded in carbon for stub hole 1

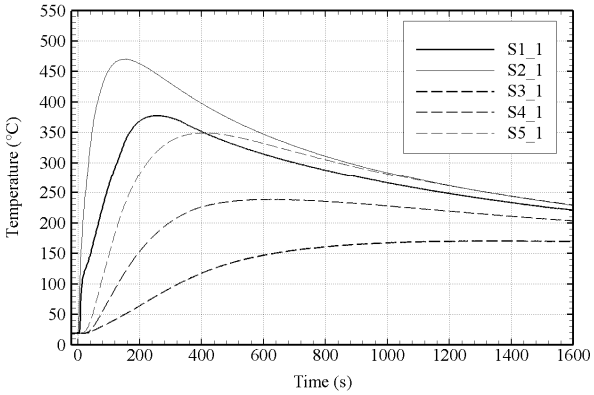

Figure 8 : First half hour of the temperatures recorded in steel for stub hole 1

Cast Iron Metallography

Cast iron samples have been cut off the thimbles to perform metallographic analysis. The samples were cut to observe the microstructure at the corresponding location of TCs I1, I2, I3 and I4 in the stub hole number 1. The results presented here come from optical microscopy without etching. Further analysis with microprobe will be performed later to observe the matrix composition and alloying elements. It will then be possible to make more definitive statements on the phase changes observed in the cooling curves.

Figure 9 to Figure 12 represent the microstructure from the thicker to the thinner section, corresponding to TCs I3, I4, I1 and I2 respectively. There is an obvious evolution in the microstructure as a function of the cooling rate. The slowest one resulted in a dendritic structure and the fastest one gave graphite flakes. The two intermediate cooling rates yielded a hybrid structure made of dendrites and finer flakes.

Figure 9 : Microstructure of the cast iron at TC I3 location

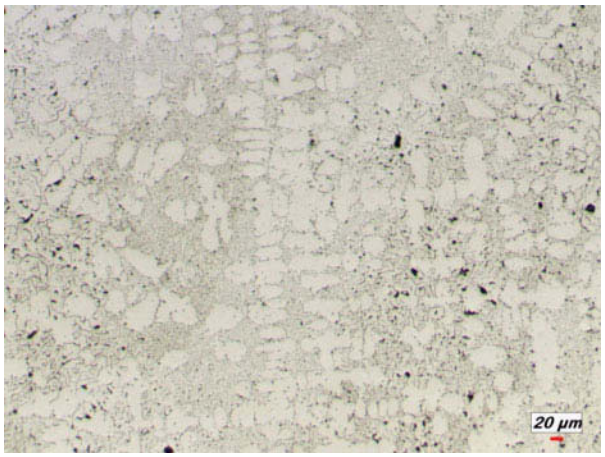

Figure 10 : Microstructure of the cast iron at TC I4 location

Figure 11 : Microstructure of the cast iron at TC I1 location

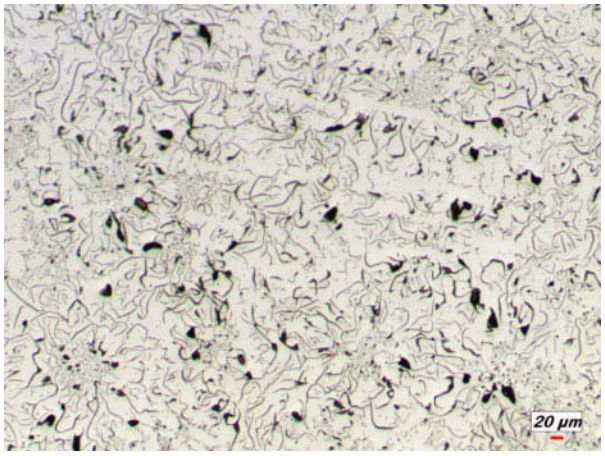

Figure 12 : Microstructure of the cast iron at TC I2 location

Interface Heat Transfer Coefficient

In order to evaluate the HTCs at the casting interfaces, a 3D thermal model was built in Abaqus. The HTCs were imposed through a GapCond subroutine in which a particular relation was applied to each contact interfaces. Based on the work of Trovant and Argyropoulos[10, 11] with a casting in a sand mould, the HTC at the carbon/cast iron interface is expected to drop rapidly in the first seconds of the casting and then slowly decrease because the air gap opens. For this reason, the chosen form for the HTC relation is:

(2)

The relation depends on time. A, B and C are parameters identified with a trial and error method by running the model several times until the cooling curves closely match the 39 experimental curves. Table 1 shows the final parameters obtained with the model and Figure 13 shows the curve fitting at four TCs locations.

Table 1 : Parameters identified in equation (2) for the heat transfer coefficients at the casting interfaces

Interface	A	B	C
Carbon/Cast Iron	400	0.0005	400
Steel/Cast Iron	350	0.00001	600
Carbon/Steel	325	0.0005	400

Because of its very small parameter B, the HTC at the steel/cast iron interface decreases slower (almost linearly) than the carbon/cast iron one. The cast iron shrinks around the stub as it cools down, hence the interface pressure rises. It helps maintain a good contact and heat transfer.

One drawback of this method is that the HTCs can not be related to the air gap opening at the carbon/cast iron interface or to the pressure at the steel/cast iron interface. A thermo-mechanical solidification model that is currently developed to predict the air gap would have been of great use to better evaluate HTCs with rather physical relations to gap opening or surface pressure than time, but the model is not advanced enough to accomplish this task due to convergence problems with viscoplastic and damage issues. However, the current relation still gives valuable information.

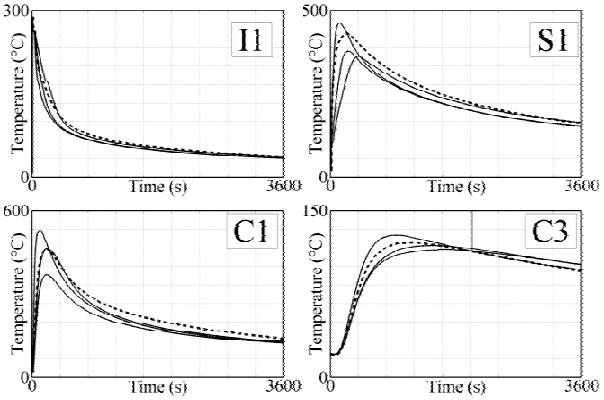

Figure 13 : First hour of the thermal model cooling curves (dashed) against TCs cooling curves from the three stub holes

Conclusion

The results of an experimental investigation of the sealing of an anode assembly have been presented in order to provide information for the validation of a thermo-mechanical solidification model to predict the air gap at the carbon/cast iron interface.

It was found that the relation previously proposed by Richard (Equation (1)) underestimates the magnitude of the air gap at the carbon/cast iron interface. Given that many works have used this relation to evaluate an initial air gap condition, it is suggested that the results of these works be reevaluated with the new available data.

Cooling curves recorded with thermocouples during the sealing of an anode assembly allowed observation of the thermal field as a function of time. Those curves will be useful for the validation of a thermo-mechanical solidification model to predict the air gap.

From the cooling curves, it was possible to evaluate the heat transfer coefficient at the interfaces with a 3D thermal model. The coefficients found here are functions of time and are therefore only good as a guideline for modeling. It should be considered to carry out real time air gap measurements with LVDTs in conjunction with thermocouples in order not only to better evaluate the heat transfer coefficients, but also to have a better understanding of the strains as the cast iron cools down with the help of the forthcoming thermo-mechanical model.

It was also possible to observe the importance of the effect of cooling rate on the final microstructure of the solidified cast iron through metallographic analysis going from dendritic structure to large flakes of graphite. Still to be determined is the need to take this phenomenon into account in an air gap prediction model.

Reference [13] provides more details about the work presented in this paper.

Acknowledgments

The authors gratefully acknowledge the financial support provided by Alcoa Inc., the Natural Sciences and Engineering Research Council of Canada, the Fonds québécois de la recherche sur la nature et les technologies and the Aluminium Research Centre – REGAL. We also thank the following people for their indispensable help: Hugues Ferland, Edmond Rousseau (REGAL), Maude Larouche(Université Laval), Michel Gasse, Jean-Pierre Rapin, Daniel Lapointe (Alcoa Deschambault).

References

1. Beier, S., J. J. J. Chen, and M. Fafard, *FEM Analysis of the Anode Connection in Aluminium Reduction Cells.* Light Metals, 2011.

2. Fortin, H., *Modélisation du comportement thermo-électro-mécanique de l'anode de carbone utilisée dans la production primaire de l'aluminium*, Master Thesis, Université Laval, Québec, Canada, 2010.

3. Fortin, H., M. Fafard, N. Kandev, and P. Goulet, *FEM Analysis of Voltage Drop in the Anode Connector Assembly.* Light Metals, 2009, p. 1055-1060.

4. Richard, D., *Conception des tourillons d'anode en usage dans une cuve de Hall-Héroult à l'aide de la méthode des éléments finis*, Master Thesis, Université Laval, Québec, Canada, 2000.

5. Richard, D., P. Goulet, O. Trempe, M. Dupuis, and M. Fafard, *Challenges in Stub Hole Optimisation of Cast Iron Rodded Anodes.* Light Metals, 2009, p. 1067-1072.

6. Celentano, D., D. Gunasegaram, and T. Nguyen, *A thermomechanical model for the analysis of light alloy solidification in a composite mould.* International Journal of Solids and Structures, 1999. **36**(16), p. 2341-2378.

7. Coates, B. and S.A. Argyropoulos, *The effects of surface roughness and metal temperature on the heat-transfer coefficient at the metal mold interface.* Metallurgical and Materials Transactions B, 2007. **38**(2), p. 243-255.

8. Grandfield, J., D. Mortensen, H. Fjaer, P. Rohan, V. Nguyen, H. Sund, and T. Nguyen, *Remelt ingot mold heat flow and deformation.* Light Metals, 2006, p. 869-876.

9. Gunasegaram, D.R. and T.T. Nguyen, *Effect of cooling rate on air gap formation in aluminium alloy permanent mould casting.* International Journal of Cast Metals Research, 2006. **19**(2), p. 116-122.

10. Trovant, M. and S. Argyropoulos, *Finding boundary conditions: A coupling strategy for the modeling of metal casting processes: Part I. Experimental study and correlation development.* Metallurgical and Materials Transactions B, 2000. **31**(1), p. 75-86.

11. Trovant, M. and S. Argyropoulos, *Finding boundary conditions: A coupling strategy for the modeling of metal casting processes: Part II. Numerical study and analysis.* Metallurgical and Materials Transactions B, 2000. **31**(1), p. 87-96.

12. Vicente-Hernandez, P., F. Decultieux, P. Schmidt, I.L. Svensson, and C. Levaillant, *Mushy State Behavior - Rheological Characterization and Influence on Air-Gap Formation.* Isij International, 1995. **35**(6), p. 805-812.

13. Trempe, O., *Étude expérimentale et modélisation du scellement d'un ensemble anodique d'une cuve Hall-Héroult*, Master Thesis, Université Laval, Québec, Canada, 2011.